Geom Dedicata (2015) 177:103–128
DOI 10.1007/s10711-014-9981-3

ORIGINAL PAPER

Closed-form characterization of the Minkowski sum and difference of two ellipsoids

Yan Yan · Gregory S. Chirikjian

Received: 12 June 2013 / Accepted: 8 April 2014 / Published online: 22 April 2014

Abstract This paper makes three original contributions: (1) Explicit closed-form parametric formulas for the boundary of the Minkowski sum and difference of two arbitrarily oriented solid ellipsoids in n-dimensional Euclidean space are presented; (2) Based on this, new closed-form lower and upper bounds for the volume contained in these Minkowski sums and differences are derived in the 2D and 3D cases and these bounds are shown to be better than those in the existing literature; (3) A demonstration of how these ideas can be applied to problems in computational geometry and robotics is provided, and a relationship to the Principal Kinematic Formula from the fields of integral geometry and geometric probability is uncovered.

Keywords Minkowski sum · Ellipsoid · Integral geometry · Steiner's formula · Mean curvature

Mathematics Subject Classification 65Dxx

1 Introduction

The Minkowski sum of two convex point sets (or bodies) centered at the origin, C_1 and C_2 in $\mathbb{R}^n$, is denoted by $C_1 \oplus C_2$ and is defined as

$$C_1 \oplus C_2 \doteq \{p_1 + p_2 \mid p_1 \in C_1, p_2 \in C_2\}. \tag{1}$$

The Minkowski difference between C_1 and C_2, denoted by $C_1 \ominus C_2$, is defined as [48]

$$C_1 \ominus C_2 \doteq \bigcap_{p_2 \in C_2} (C_1 + p_2), \tag{2}$$

Y. Yan · G. S. Chirikjian (✉)
Department of Mechanical Engineering, Johns Hopkins University, Baltimore, MD21218, USA
e-mail: gchirik@gmail.com

Y. Yan
e-mail: yyan@jhu.edu

Alternatively, by the definition of the Minkowski sum, we can define the Minkowski difference of two convex bodies as $C_1 \ominus C_2 = C_1'$, where $C_1 = C_1' \oplus C_2$.

Minkowski operations are used in a wide range of applications such as robot motion planning [33], CAD/CAM, assembly planning [25] and computer-aided design [26]. For example, consider an obstacle P and a robot Q that moves by translation. If we choose a reference point attached to Q, then $P \oplus Q$ is the locus of positions of the reference point where $P \cap Q \neq \emptyset$. In the study of motion planning this sum is called a configuration space obstacle. Alternatively, if P is an arena in which the robot Q is confined to move, then $P \ominus Q$ is the locus of positions of the reference point where $P \cap Q = Q$, and represents the robot's collision-free configuration space with respect to the arena.

While defining the Minkowski operations mathematically is easy, computing useful representations of Minkowski sums or differences can be difficult and computationally expensive, especially when the exact boundary of the resulting objects needs to be represented explicitly. Much work has been done on obtaining boundaries of the Minkowski sums of two sets in two and three dimensions and on developing fast algorithms for computing Minkowski sums numerically [5]. The Minkowski sums of polygons (for two-dimensional cases) and polyhedra (for three-dimensional cases) have been extensively studied in the computational geometry literature [2,14,22,23,26]. The related algorithms are mainly based on either the computation of the convolution of geometric boundaries [22], or polygon/polyhedra decompositions [2,14,23,26]. Minkowski sums of curved regions/surfaces have also been studied (e.g. [4,28,34,41]).

Motivated by the robot motion planning problem using ellipsoidal bounding boxes, we present an approach to parameterizing the exact Minkowski sum and difference of two solid ellipsoidal bodies in closed form. The Minkowski sum can be computed numerically by rapidly determining when two particular ellipsoidal bodies at given center positions and orientations intersect or not [3,10,19,36], or by ellipsoidal calculus [31,32,40]. However, the exact closed-form characterization of this fundamental result appears not to have been reported elsewhere in the literature. The basic idea of our approach is to use a combination of affine transformations together with the analytic properties of offset surfaces to obtain an exact closed-form parametric expression for the boundary. This approach can be used for arbitrarily shaped ellipsoids (i.e., those with semi-axis lengths that can be different in each direction) with arbitrary orientations, and the methodology applies both to Minkowski sums and differences. The Minkowski sum and difference of two ellipsoidal bodies are in general not ellipsoidal. Different than most of the existing methods, our approach is completely analytical and has a closed form and therefore naturally provides improved efficiency.

The second half of the paper studies volume bounds for the Minkowski sum of two ellipsoidal bodies. With our exact parameterization, they can be calculated numerically, however, in general, formulas for the volumes enclosed in these regions do not have exact closed-form expressions. Based on Steiner's Formula, we develop an approach to provide an exact closed-form formula for the volume in the axis-symmetric 3D case, and closed-form upper and lower bounds in more general triaxial cases in 3D. We also develop related bounds in the 2D case.

The remainder of this paper is structured as follows. Section 2 parameterizes in closed form the bounding surface of the Minkowski sum and difference of two ellipsoidal bodies at arbitrary orientations in n-dimensional Euclidean space. Section 3 studies the volume enclosed in the Minkowski sum of two solid ellipsoids. An approach based on Steiner's Formula is presented to provide closed-form bounds of those volumes. These bounds and the numerically calculated ground truth are compared and analyzed for different planar elliptical and three-dimensional ellipsoidal examples. Then in Sect. 4 these results are applied to

characterize the volume of free motion of an ellipsoidal robot moving among ellipsoidal obstacles in an ellipsoidal arena. We also discuss a new extension of the Principal Kinematic Formula. Finally, Sect. 5 presents our conclusions.

2 Closed-form characterization of Minkowski operations of two ellipsoids

In this section a combination of affine transformations and the analytic properties of offset surfaces are used to obtain exact closed-form parametric expressions for the boundaries of the Minkowski sum and difference of any two ellipsoidal bodies.[1] In order to keep things general, in addition to its usual meaning, the word "ellipsoid" is used to describe an ellipse in two-dimensional space, and a hyper-ellipsoid in n-dimensional space when $n > 3$. And a "solid ellipsoid" refers to the ellipsoidal body bounded by an ellipsoid.

Let E_1 and E_2 be two arbitrary solid ellipsoids in n-dimensional Euclidean space with semi-axis lengths given by the row vectors $\mathbf{a}_1 = [a_1, \ldots, a_n]$ and $\mathbf{a}_2 = [a'_1, \ldots, a'_n]$, respectively. The ellipsoidal boundary ∂E_1 that encloses E_1 has implicit and parametric equations of the form[2]

$$\mathbf{x}^T A_1^{-2} \mathbf{x} = 1 \quad \text{and} \quad \mathbf{x} = A_1 \mathbf{u}(\phi) \tag{3}$$

where $A_1 = R_1 \Lambda(\mathbf{a}_1) R_1^T$ with R_1 denoting the $n \times n$ rotation matrix that orients E_1 in space and $\Lambda(\mathbf{a}_1) = [\lambda_{ij}(\mathbf{a}_1)]$ is the $n \times n$ diagonal matrix with entries of the form $\lambda_{ij}(\mathbf{a}_1) = a_i \, \delta_{ij}$ (no sum), where δ_{ij} is the Kronecker delta symbol and the ith semi-axis length a_i is the ith component of $\mathbf{a}_1$. Here $\mathbf{u}(\phi)$ is the standard parameterization of the hyper-sphere S^{n-1} with $n-1$ angles $\phi = [\phi_1, \ldots, \phi_{n-1}]$ as used in [12]. Subscripts on the matrices $A_i \Lambda(\mathbf{a}_i)$ and R_i refer to ellipsoid E_i.

Let E_2 translate around E_1 and attach a reference point in the center of E_2. Then the boundary of $E_1 \oplus E_2$ becomes the locus of positions of the reference point of E_2 where $E_1 \cap (t \cdot E_2) \neq \emptyset$ for all translations $t \in \mathbb{R}^n$ where $t \cdot E_2$ denotes a translated version of E_2 defined by $t \cdot E_2 = \{x + t | x \in E_2\}$.

The basic idea of our approach is to apply an affine transformation to E_1 and E_2 that results in shrinking E_2 into a ball of radius r, and calculating an offset surface of the transformed ∂E_1 with offset distance r. We then stretch the resulting offset surface using the inverse of the previous affine transformation. For a graphical explanation, this general algorithm is illustrated with a planar example in Fig. 1a–c. In Fig. 1a, the boundary of the Minkowski sum of E_1 and E_2 is constructed by the center of E_2 when it is touching E_1. It forms a deformed offset curve/surface of the motionless ellipsoid with variable offset distances. To characterize the boundary of $E_1 \oplus E_2$, first, as shown in Fig. 1b we shrink both ellipsoids together until ∂E_2 changes to a circle/sphere with radius r. Here, r is chosen as the smallest semi-axis length of E_2 i.e., $r = \min\{a'_1, a'_2, \ldots, a'_n\}$. Therefore, the boundary of $E_1 \oplus E_2$ in this case becomes an offset curve/surface. After this affine operation E_1 still remains an ellipsoid but with changed semi-axis lengths, $\tilde{a}_i$, and changed orientation.

The "shrinking" operation on E_1 can be represented as

$$\mathbf{x}' = R_2 \Lambda^{-1}(\mathbf{a}_2/r) R_2^T \mathbf{x}, \tag{4}$$

[1] In the case of the Minkowski difference, mild conditions are imposed requiring one body to be containable in the other at all orientations and under all kissing conditions.

[2] Of course the same applies for E_2 in its principal axis frame with $\mathbf{a}_1 \rightarrow \mathbf{a}_2$.

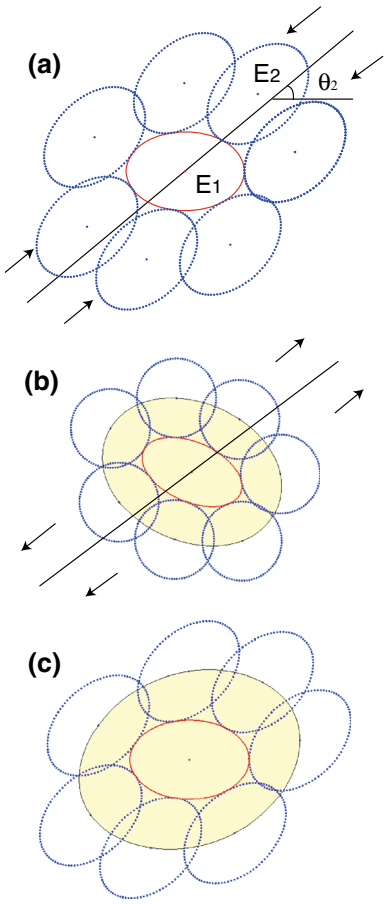

Fig. 1 The algorithm for obtaining the parametric representation of the boundary of the Minkowski sum of two elliptical bodies E_1 and E_2. In **a**, both bodies are shrunk in the direction with the rotation angle θ_2 [see (4)] until ∂E_2 becomes a circle. After the shrinking process, ∂E_1 remains elliptical but with different semi-axis lengths and rotation angle, whereas ∂E_2 becomes a circle (see **b**). The Minkowski sum in this transformed space is then an offset surface. In **c**, everything is stretched back in the same direction until the surrounding circle becomes the original version of ∂E_2 again. The *shaded region* in **c** represents $E_1 \oplus E_2$. We note that the *shaded regions* in **b**, **c** that may appear to be elliptical are actually not ellipses, and the amount that they deviate from being ellipses depends on the eccentricity of the elliptical bodies

where $\mathbf{x}$ and $\mathbf{x}'$ specify the coordinates of the original and shrunk versions of E_1, respectively. R_2 is the rotation matrix describing the orientation of E_2.

Then $\mathbf{x}$ can be represented as

$$\mathbf{x} = R_2 \Lambda(\mathbf{a}_2/r) R_2^T \mathbf{x}'. \tag{5}$$

By substituting (5) into the first equation in (3), we can get the implicit expression of the shrunk version of ∂E_1 of the form

$$\Phi(\mathbf{x}') \doteq (\mathbf{x}')^T A_1'^{-2} \mathbf{x}' = 1, \tag{6}$$

where A_1' depends on the rotation matrices R_1, R_2, and the semi-axis lengths $\mathbf{a}_1$ and $\mathbf{a}_2$.

A parameterized offset hyper-surface $\mathbf{x}_{ofs}(\phi)$ of an orientable, closed, and differentiable hyper-surface $\mathbf{x}'(\phi) \in \mathbb{R}^n$ with the offset radius r is defined as

$$\mathbf{x}_{ofs}(\phi) = \mathbf{x}'(\phi) + r\,\mathbf{n}'(\phi), \tag{7}$$

where $\mathbf{n}'$ is the outward-pointing unit surface normal. In the case of the ellipsoidal surface in (6), the outward pointing normal can first be computed from the implicit equation as

$$\nabla\Phi(\mathbf{x}') = 2A_1'^{-2}\mathbf{x}'$$

and then evaluated with the parametric equation and normalized as

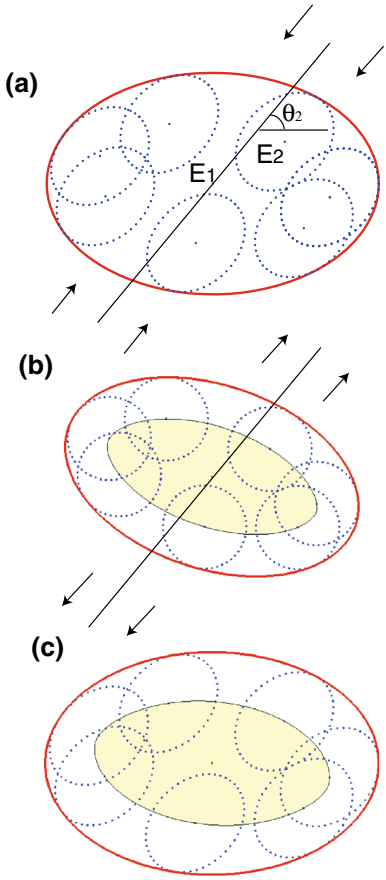

Fig. 2 The algorithm for obtaining the parametric representation of the boundary of the Minkowski difference of two solid ellipses E_1 and E_2. This presumes that the radius of curvature of the resulting *circle/sphere* is smaller than the smallest semi-axis length of the bounding shrunk ellipsoid. The algorithm follows the same steps as Fig. 1. The *shaded region* in **c** represents $E_1 \ominus E_2$

$$\mathbf{n}'(\phi) = \frac{\nabla \Phi(\mathbf{x}'(\phi))}{\|\nabla \Phi(\mathbf{x}'(\phi))\|} \tag{8}$$

where $\mathbf{x}'(\phi) = A_1' \mathbf{u}(\phi)$ is analogous to the parametric expression on the right side of (3).

Substituting this into (7) gives a closed-form expression for the offset of the affine-transformed version of ∂E_1. After computing the offset hyper-surface $\mathbf{x}_{ofs}$, we just need to transform the result back until the shrunk version of E_1 becomes to the original one again (see Fig. 1c), and after this "stretching" operation, the exact boundary of $E_1 \oplus E_2$ can be finally represented in closed form as

$$\mathbf{x}_{eb} = T \mathbf{x}_{ofs} \quad \text{where} \quad T = R_2 \Lambda(\mathbf{a}_2 / r) R_2^T . \tag{9}$$

The boundary of the Minkowski difference of two ellipoids E_1 and E_2 is denoted as $\partial(E_1 \ominus E_2)$. When E_2 is "small enough" relative to $E_1 \partial(E_1 \ominus E_2)$ can be parameterized in exactly the same way as above for $\partial(E_1 \oplus E_2)$, with the single change that in (7) $r \to -r$. Here "small enough" means that at any orientation a translate of ∂E_2 can simultaneously kiss ∂E_1 at a single point and be fully contained in E_1. This amounts to the maximal radius of curvature of ∂E_2 to be less than the minimal radius of curvature of ∂E_1.

The procedure for generating the boundary of the Minkowski difference is illustrated in Fig. 2.

3 Volume of the Minkowski sum of two ellipsoids

Here we show that using the methods developed in the previous section it is possible to approximate the volume of the Minkowski sum of two arbitrary ellipsoidal bodies with lower bounds that are tighter than the *Brunn–Minkowski* inequality

$$V(E_1 \oplus E_2)^{\frac{1}{n}} \geq V(E_1)^{\frac{1}{n}} + V(E_2)^{\frac{1}{n}}. \tag{10}$$

Moreover, using similar methods, we can also generate tight upper bounds. The bounds that we develop in this section use Steiner's formula [43,47]

$$V\left(C \oplus r \cdot B^n\right) = W_0(C) + \sum_{k=1}^{n} \binom{n}{k} W_k(C) r^k \tag{11}$$

where C is an arbitrary convex body and B^n is a unit ball in $\mathbb{R}^n r$ is a radius and $W_i(C)$ is the ith *quermassintegral*. In the current context, C is the interior of an n-dimensional ellipsoid, which is an affine transformed version of the original E_1, and $r \cdot B^n$ is the solid ball resulting from the same affine transformation applied to E_2. The affine transformation that transforms $r \cdot B^n$ back into E_2 is defined by its action on an arbitrary point $\mathbf{x} \in \mathbb{R}^n$ into $T\mathbf{x}$ where T is the $n \times n$ matrix in (9) with $\det T > 0$. The volume $V(C \oplus r \cdot B^n)$ is then related to $V(E_1 \oplus E_2)$ by the formula

$$V(E_1 \oplus E_2) = \det(T) \cdot V(C_r) \tag{12}$$

where the shorthand

$$C_r \doteq C \oplus r \cdot B^n$$

is used here and in the subsequent subsections. Even though the boundary is parameterized in closed form, not all of the quermassintegrals can be evaluated in closed form. However, we show in the following subsections that they can all be bounded well in 2D and in 3D.

For the Minkowski difference, the same formula can be used with $r \to -r$ under the same relative size conditions on E_1 and E_2 as in the previous section. These conditions amount to the smallest radius of curvature of ∂E_1 being larger than the largest radius of curvature of ∂E_2, with this comparison being performed over all points on both bodies.

3.1 Volumes of offsets via Steiner's formula (planar case)

In the planar case, Steiner's Formula becomes[3]

$$V(C_r) = V(C) + rL(\partial C) + \pi r^2, \tag{13}$$

where $L(\partial C)$ represents the perimeter of the ellipse. The perimeter of an ellipse with semi-axis lengths a and b with $a \leq b$ can be written exactly as

$$L(a, b) = 4b\, E\left(\frac{\pi}{2}, \sqrt{1 - \frac{a^2}{b^2}}\right) \tag{14}$$

where $E(\varphi, m)$ is the incomplete elliptic integral of the second kind. Using this, the exact area contained inside of the offset curve can be obtained, and the exact area of the Minkowski

[3] Since area takes the place of volume in 2D problems, and we retain the symbol V when referring to area.

sum of two ellipses results. Nevertheless, it can be useful to evaluate lower and upper bounds using elementary functions.

The perimeter of an ellipse can be approximated by Legendre's exact expansion [35],

$$L(a,b) = 2\pi a\left[1 - \frac{w^2}{4} - \frac{3w^4}{64} - (2\nu-1)^{-1}\left(2\nu\nu\right)^2\left(\frac{w}{4}\right)^{2\nu} - \cdots\right], \tag{15}$$

where w is the eccentricity of the ellipse, i.e., with $a \geq b$,

$$w = \sqrt{1 - \frac{b^2}{a^2}}. \tag{16}$$

Therefore, we can use the first few terms as an upper bound, for example

$$L_{ub} = 2\pi a\left(1 - \frac{w^4}{4} - \frac{3w^2}{64}\right). \tag{17}$$

Also, by the isoperimetric inequality [30], we have a lower bound of L as

$$L_{lb} = \sqrt{4\pi^2 ab + 4\pi(a-b)^2}. \tag{18}$$

3.2 Volumes of offsets via Steiner's formula (spatial case)

For a finite convex 3D body C with volume $V(C)$ enclosed by a compact surface ∂C, Steiner's formula calculates the volume enclosed by the surface offset by an amount r from ∂C [24]:

$$V(C_r) = V(C) + rF(\partial C) + r^2 M(\partial C) + \frac{r^3}{3}K(\partial C). \tag{19}$$

Here $F(\partial C)$ is the area of the bounding surface, $M(\partial C)$ is the mean curvature integrated over the bounding surface, and $K(\partial C)$ is the Gaussian curvature integrated over the bounding surface. From the Gauss–Bonnet theorem applied to the surface bounding a simply-connected body (as must be the case for a convex body),

$$K(\partial C) = 4\pi. \tag{20}$$

and so, if the surface area and integral of mean curvature can be computed, we can exactly compute the volume of the offset surface.

This, together with (12) and our construction of the Minkowski sum of ellipsoids by the application of appropriate linear transformations resulting in offset surfaces of ellipsoids, allows us to bound the volume of the Minkowski sum of ellipsoids in closed form. Here we seek to bound these quantities from below and above, thereby bounding the volume of the offset of an ellipse, and from our previous construction, bounding the volume of the Minkowski sum of two arbitrary ellipsoids at arbitrary orientations.

In the spatial case, both the surface area and mean curvature must either be computed, bounded, or approximated.

3.2.1 Total mean curvature

Exact formulas are not known to us for the total mean curvature M, for a triaxial ellipsoid. But several approaches to bounding this quantity are possible.

Given the parameterized equation of a triaxial ellipsoid

$$\mathbf{x}(\phi,\theta)=\begin{pmatrix} a\cos\phi\sin\theta \\ b\sin\phi\sin\theta \\ c\cos\theta \end{pmatrix}$$

the outward pointing normal is

$$\begin{aligned}\mathbf{n}(\phi,\theta)&=\left(\frac{\partial\mathbf{x}}{\partial\theta}\times\frac{\partial\mathbf{x}}{\partial\phi}\right)\cdot\left\|\frac{\partial\mathbf{x}}{\partial\theta}\times\frac{\partial\mathbf{x}}{\partial\phi}\right\|^{-1}\\&=\begin{pmatrix} bc\cos\phi\sin\theta \\ ac\sin\phi\sin\theta \\ ab\cos\theta \end{pmatrix}\cdot\left(b^2c^2\cos^2\phi\sin^2\theta+a^2c^2\sin^2\phi\sin^2\theta+a^2b^2\cos^2\theta\right)^{-1/2}\end{aligned}$$

Therefore,

$$\mathbf{x}\cdot\mathbf{n}=abc\cdot\left(b^2c^2\cos^2\phi\sin^2\theta+a^2c^2\sin^2\phi\sin^2\theta+a^2b^2\cos^2\theta\right)^{-1/2}$$

and the element of surface area is

$$\begin{aligned}dS&=\left\|\frac{\partial\mathbf{x}}{\partial\theta}\times\frac{\partial\mathbf{x}}{\partial\phi}\right\|d\phi d\theta \\&=\left(b^2c^2\cos^2\phi\sin^2\theta+a^2c^2\sin^2\phi\sin^2\theta+a^2b^2\cos^2\theta\right)^{1/2}\sin\theta d\phi d\theta.\end{aligned}\tag{21}$$

In general, the mean curvature can be computed using the formula [17]

$$\begin{aligned}m&=\frac{\|\nabla\Phi\|^2\operatorname{tr}(\nabla\nabla^T\Phi)-(\nabla^T\Phi)(\nabla\nabla^T\Phi)(\nabla\Phi)}{2\|\nabla\Phi\|^3}\\&=\nabla\cdot\left(\frac{\nabla\Phi}{\|\nabla\Phi\|}\right).\end{aligned}\tag{22}$$

For the triaxial ellipsoid

$$\Phi(\mathbf{x})\doteq\mathbf{x}^T A\,\mathbf{x}\tag{23}$$

with

$$A=\Delta^{-1}(a^2,b^2,c^2),\tag{24}$$

we evaluate at $\mathbf{x}=\mathbf{x}(\phi,\theta)$ (using the same parametric equation above), which gives

$$\begin{aligned}m(\phi,\theta)&=\frac{\left(\mathbf{x}^TA^2\,\mathbf{x}\right)\,\operatorname{tr}(A)-\mathbf{x}^TA^3\,\mathbf{x}}{2\cdot\left(\mathbf{x}^TA^2\,\mathbf{x}\right)^{3/2}}\\&=\frac{abc\left[(a^2+b^2)\cos^2\theta+\left((a^2+c^2)\sin^2\phi+(b^2+c^2)\cos^2\phi\right)\sin^2\theta\right]}{2(a^2b^2\cos^2\theta+c^2(b^2\cos^2\phi+a^2\sin^2\phi)\sin^2\theta)^{3/2}}\end{aligned}\tag{25}$$

The total mean curvature of a triaxial ellipsoid is

$$\begin{aligned}M&=\int_{\partial C}m\,dS\\&=\int_0^{\pi}\int_0^{2\pi}\frac{abc\left[(a^2+b^2)\cos^2\theta+\left((a^2+c^2)\sin^2\phi+(b^2+c^2)\cos^2\phi\right)\sin^2\theta\right]}{2\left(a^2b^2\cos^2\theta+c^2\left(b^2\cos^2\phi+a^2\sin^2\phi\right)\sin^2\theta\right)}\sin\theta d\phi d\theta.\end{aligned}\tag{26}$$

We note that the fractional power disappeared due to the product of $m \cdot dS$.

One approach to obtain bounds for M is to tackle the problem by integrating M over ϕ first. In order to simplify the discussion, we denote

$$\begin{aligned} k_0 &= \frac{abc}{2}, \\ k_1(\theta) &= \left[(a^2+c^2)\sin^2\theta + (a^2+b^2)\cos^2\theta\right]\sin\theta, \\ k_2(\theta) &= \left[(b^2+c^2)\sin^2\theta + (a^2+b^2)\cos^2\theta\right]\sin\theta, \\ h_1(\theta) &= \left(a^2b^2\cos^2\theta + a^2c^2\sin^2\theta\right)^{1/2}, \\ h_2(\theta) &= \left(a^2b^2\cos^2\theta + b^2c^2\sin^2\theta\right)^{1/2}. \end{aligned} \tag{27}$$

and M in (26) can be rewritten as

$$M = k_0 \int_0^{\pi}\int_0^{2\pi} \frac{k_1(\theta)\sin^2\phi + k_2(\theta)\cos^2\phi}{h_1^2(\theta)\sin^2\phi + h_2^2(\theta)\cos^2\phi}\, d\phi d\theta. \tag{28}$$

We integrate M over ϕ first,

$$\begin{aligned} &\int_0^{2\pi} \frac{k_1(\theta)\sin^2\phi + k_2(\theta)\cos^2\phi}{h_1^2(\theta)\sin^2\phi + h_2^2(\theta)\cos^2\phi}\, d\phi \\ &\quad = 2\pi\left(\frac{k_1(\theta)}{h_1(\theta)(h_1(\theta)+h_2(\theta))} + \frac{k_2(\theta)}{h_2(\theta)(h_1(\theta)+h_2(\theta))}\right). \end{aligned} \tag{29}$$

Since

$$\begin{aligned} \int_0^{\pi/2} \frac{\cos^2 x\, dx}{\alpha^2\sin^2 x + \beta^2\cos^2 x} &= \frac{\pi}{2\beta(\alpha+\beta)}, \\ \int_0^{\pi/2} \frac{\sin^2 x\, dx}{\alpha^2\sin^2 x + \beta^2\cos^2 x} &= \frac{\pi}{2\alpha(\alpha+\beta)}, \end{aligned}$$

moreover, a general principle is that if

$$A = \int_0^{\pi/2} f(\cos^2 x, \sin^2 x)dx \ \text{ and } \ B = \int_0^{\pi/2} f(\sin^2 x, \cos^2 x)dx$$

then

$$\int_0^{\pi} f(\cos^2 x, \sin^2 x)dx = A + B \ \text{ and } \ \int_0^{2\pi} f(\cos^2 x, \sin^2 x)dx = 2(A+B),$$

and so

$$\int_0^{2\pi} \frac{\cos^2 x\, dx}{\alpha^2 \sin^2 x + \beta^2 \cos^2 x} = \frac{2\pi}{\beta(\alpha+\beta)},$$
$$\int_0^{2\pi} \frac{\sin^2 x\, dx}{\alpha^2 \sin^2 x + \beta^2 \cos^2 x} = \frac{2\pi}{\alpha(\alpha+\beta)}.$$

Then M becomes

$$M = 2k_0\pi \int_0^{\pi} \left(\frac{k_1(\theta)}{h_1(\theta)(h_1(\theta)+h_2(\theta))} + \frac{k_2(\theta)}{h_2(\theta)(h_1(\theta)+h_2(\theta))} \right) d\theta, \tag{30}$$

in which

$$\int_0^{\pi} \frac{k_1(\theta)}{h_1(\theta)(h_1(\theta)+h_2(\theta))} d\theta \tag{31}$$
$$= \int_{-1}^{1} \frac{\alpha_1 t^2 + \beta_1}{\sqrt{\alpha_2 t^2 + \beta_2}\left(\sqrt{\alpha_2 t^2 + \beta_2} + \sqrt{\alpha_3 t^2 + \beta_3}\right)} dt.$$

where

$$\begin{aligned} \alpha_1 &= b^2 - c^2, \\ \alpha_2 &= a^2\left(b^2 - c^2\right), \\ \alpha_3 &= b^2\left(a^2 - c^2\right), \\ \beta_1 &= a^2 + c^2, \\ \beta_2 &= a^2 c^2, \\ \beta_3 &= b^2 c^2. \end{aligned} \tag{32}$$

We can bound the term $\sqrt{(\alpha_2 t^2 + \beta_2)(\alpha_3 t^2 + \beta_3)}$ as

$$\alpha' t^2 + \beta' \le \sqrt{\left(\alpha_2 t^2 + \beta_2\right)\left(\alpha_3 t^2 + \beta_3\right)} \le \alpha'' t^2 + \beta'' \tag{33}$$

and in this way, replace the denominators with $\alpha' t^2 + \beta'$ and $\alpha'' t^2 + \beta''$, and bounding integrals that can be computed in closed form.

To get (α', β') and (α'', β''), first we expand out

$$\left(\alpha_2 t^2 + \beta_2\right)\left(\alpha_3 t^2 + \beta_3\right) = (\alpha_2\alpha_3)\, t^4 + (\alpha_2\beta_3 + \alpha_3\beta_2)\, t^2 + \beta_2\beta_3.$$

Next, compare with a candidate perfect square

$$(\alpha t^2 + \beta)^2 = \alpha^2 t^4 + 2\alpha\beta t^2 + \beta^2.$$

We have complete control over defining $\alpha, \beta \in \mathbb{R}_{\ge 0}$, and want to choose them so that one of the results $(\alpha t^2 + \beta)^2 \le (\alpha_2 t^2 + \beta_2)(\alpha_3 t^2 + \beta_3)$ or $(\alpha t^2 + \beta)^2 \ge (\alpha_2 t^2 + \beta_2)(\alpha_3 t^2 + \beta_3)$ holds, and is as tight as we can make it.

If we choose

$$\beta^2 \doteq \beta_2\beta_3 \quad \text{and} \quad 2\alpha\beta \doteq \alpha_2\beta_3 + \alpha_3\beta_2$$

then the difference

$$(\alpha t^2+\beta)^2-(\alpha_2 t^2+\beta_2)(\alpha_3 t^2+\beta_3)=t^4\frac{(\beta_2\alpha_3-\beta_3\alpha_2)^2}{4\beta_2\beta_3}\geq 0.$$

And since t^4 is very small on much of the range $-1\leq t\leq 1$, using this fact will result in a good upper bound of the form

$$\sqrt{(\alpha_2 t^2+\beta_2)(\alpha_3 t^2+\beta_3)}\ \leq\ \alpha'' t^2+\beta''$$

as in the right-hand side of (33), where

$$\beta''\doteq\sqrt{\beta_2\beta_3}\quad\text{and}\quad\alpha''\doteq\frac{\alpha_2\beta_3+\alpha_3\beta_2}{2\sqrt{\beta_2\beta_3}}.$$

As for a lower bound, if we define $\alpha^2\doteq\alpha_2\alpha_3$ and $\beta^2\doteq\beta_2\beta_3$ then

$$(\alpha t^2+\beta)^2=(\alpha_2\alpha_3)t^4+2\sqrt{\alpha_2\alpha_3\beta_2\beta_3}\,t^2+\beta_2\beta_3. \tag{34}$$

But from the AM-GM inequality

$$\frac{a+b}{2}\geq\sqrt{ab},$$

it follows that the middle term in (34) is less than $\alpha_2\beta_3+\alpha_3\beta_2$. And so

$$(\alpha' t^2+\beta')^2\leq\left(\alpha_2 t^2+\beta_2\right)\left(\alpha_3 t^2+\beta_3\right)$$

where

$$\alpha'\doteq\sqrt{\alpha_2\alpha_3}\quad\text{and}\quad\beta'\doteq\sqrt{\beta_2\beta_3}$$

give the constants so that the lower bound in (33) holds.

Therefore, we have

$$\begin{aligned}\int_{-1}^{1}\frac{\alpha_1 t^2+\beta_1}{(\alpha_2+\alpha')t^2+(\beta_2+\beta')}\,dt&\leq\int_0^{\pi}\frac{k_1(\theta)}{h_1(\theta)\,(h_1(\theta)+h_2(\theta))}\,d\theta,\\ \int_0^{\pi}\frac{k_1(\theta)}{h_1(\theta)(h_1(\theta)+h_2(\theta))}\,d\theta&\leq\int_{-1}^{1}\frac{\alpha_1 t^2+\beta_1}{(\alpha_2+\alpha'')t^2+(\beta_2+\beta'')}\,dt.\end{aligned} \tag{35}$$

In the same way,

$$\begin{aligned}\int_{-1}^{1}\frac{\alpha_4 t^2+\beta_4}{(\alpha_3+\alpha')t^2+(\beta_3+\beta')}\,dt&\leq\int_0^{\pi}\frac{k_2(\theta)}{h_2(\theta)\,(h_1(\theta)+h_2(\theta))}\,d\theta,\\ \int_0^{\pi}\frac{k_2(\theta)}{h_2(\theta)\,(h_1(\theta)+h_2(\theta))}\,d\theta&\leq\int_{-1}^{1}\frac{\alpha_4 t^2+\beta_4}{(\alpha_3+\alpha'')t^2+(\beta_3+\beta'')}\,dt.\end{aligned} \tag{36}$$

From these observations, we can bound M from below and above with integrals that can be computed in closed form as

$$M_{lb1} = 4\pi \left(\frac{\alpha_1}{\alpha_2 + \alpha'} - \frac{(\alpha_1(\beta_2 + \beta') - \beta_1(\alpha_2 + \alpha')) \tan^{-1}(\sqrt{\frac{\alpha_2+\alpha'}{\beta_2+\beta'}})}{(\alpha_2 + \alpha')\sqrt{(\alpha_2 + \alpha')(\beta_2 + \beta')}} \right.$$
$$\left. + \frac{\alpha_4}{\alpha_3 + \alpha'} - \frac{(\alpha_4(\beta_3 + \beta') - \beta_4(\alpha_3 + \alpha')) \tan^{-1}(\sqrt{\frac{\alpha_3+\alpha'}{\beta_3+\beta'}})}{(\alpha_3 + \alpha')\sqrt{(\alpha_3 + \alpha')(\beta_3 + \beta')}} \right), \tag{37}$$

$$M_{ub1} = 4\pi \left(\frac{\alpha_1}{\alpha_2 + \alpha''} - \frac{(\alpha_1(\beta_2 + \beta'') - \beta_1(\alpha_2 + \alpha'')) \tan^{-1}(\sqrt{\frac{\alpha_2+\alpha''}{\beta_2+\beta''}})}{(\alpha_2 + \alpha'')\sqrt{(\alpha_2 + \alpha'')(\beta_2 + \beta'')}} \right. \tag{38}$$
$$\left. + \frac{\alpha_4}{\alpha_3 + \alpha''} - \frac{(\alpha_4(\beta_3 + \beta'') - \beta_4(\alpha_3 + \alpha'')) \tan^{-1}(\sqrt{\frac{\alpha_3+\alpha''}{\beta_3+\beta''}})}{(\alpha_3 + \alpha'')\sqrt{(\alpha_3 + \alpha'')(\beta_3 + \beta'')}} \right).$$

We now explore a second set of bounds on M for triaxial ellipsoids. Since the total mean curvature of uniaxial ellipsoids is known as exact expressions in both the prolate and oblate cases, by inscribing and circumscribing the tightest uniaxial ellipsoids around a given triaxial ellipsoid, we can obtain bounds on M of the form

$$M_{lb2} \leq M(\partial C) \leq M_{ub2} \tag{39}$$

The explicit formulas for the total mean curvature of uniaxial ellipsoids are given below. If $a = b = R$ and $c = \lambda R$ with $0 < \lambda < 1$, then [24]

$$M = 2\pi R \left[\lambda + \frac{\arccos\lambda}{\sqrt{1 - \lambda^2}} \right]. \tag{40}$$

When $\lambda > 1$,

$$M = 2\pi R \left[\lambda + \frac{\log(\lambda + \sqrt{\lambda^2 - 1})}{\sqrt{\lambda^2 - 1}} \right]. \tag{41}$$

To circumscribe a tight uniaxial ellipsoid around a given triaxial ellipsoid with $a \leq b \leq c$, we stretch the triaxial ellipsoid along the x-axis until the semi-axis length changes from a to b, or we can stretch it along the y-axis until the semi-axis length changes from b to c. The tightest circumscribed uniaxial ellipsoid can be chosen as the one with the smallest M and this M (denoted as M_{ub2} in this method) provides an upper bound of the M of the triaxial ellipsoid.

We can inscribe a uniaxial ellipsoid into the triaxial ellipsoid in the similar way by shrinking it along the z-axis until the semi-axis length changes from c to b and the M of this uniaxial ellipsoids provides a lower bound of the M of the triaxial ellipsoid. However, we notice that an even tighter lower bound can be found by using the "Schwartz-symmetrized"-version of the triaxial ellipsoid instead of a fully inscribed version. The "Schwartz-symmetrized"-version of a convex body C, denoted as C^* can be generated by condensing C into circular cross sections along an axis through the center of C. Each line keeps its original area, and so $V(C) = V(C^*)$. By the fact of $M(C^*) \leq M(C)$, we can obtain a lower bound of M and it is tighter than the one from the inscribed ellipsoid. For our ellipsoidal case, we can just let the semi-axis lengths of the "Schwartz-symmetrized" version of the triaxial ellipsoid either be $a^* = a, b^* = c^* = \sqrt{bc}$ or $a^* = b^* = \sqrt{ab} = c$ and the one with larger M is chosen as the lower bound of the M (denoted as M_{lb2}).

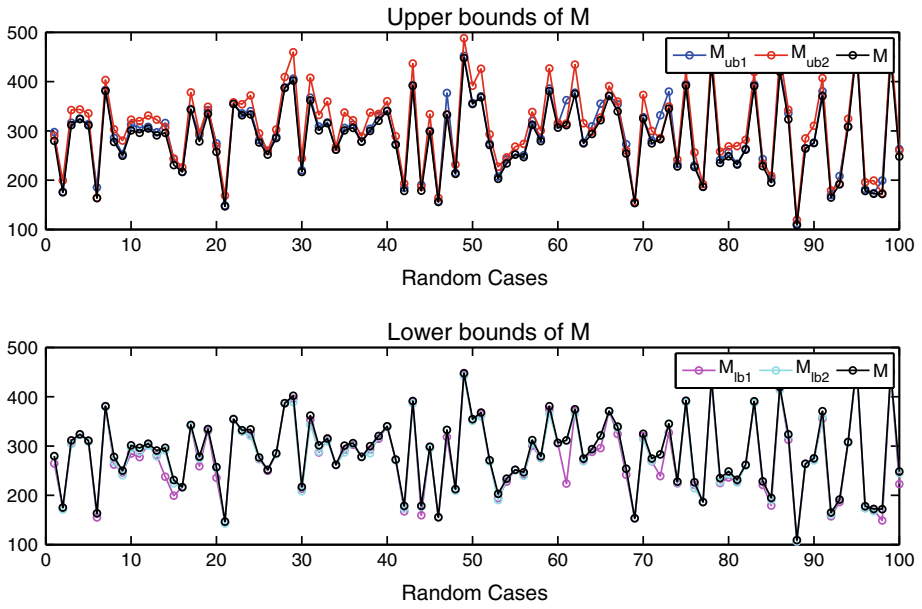

Fig. 3 *Upper* and *lower bounds*, M_{ub1}, $M_{ub2}M_{lb1}$ and M_{lb1}, are compared with the exact values of M in 100 random trials, in which the semi-axis lengths and rotation angles of the ellipsoids are randomly sampled from uniform distributions $U[10, 50]$ and $U[0, 2\pi]$, respectively

In practice, we choose the tightest bounds as our bounds of M, i.e.,

$$\begin{aligned} M_{lb} &= \max\{M_{lb1}, M_{lb2}\}, \\ M_{ub} &= \min\{M_{ub1}, M_{ub2}\}. \end{aligned} \tag{42}$$

To better illustrate different bounds of M, we use 100 random trials, in which the semi-axis lengths and rotation angles of the ellipsoids are randomly sampled from uniform distributions $U[10, 50]$ and $U[0, 2\pi]$, respectively. The results of $M_{ub1}M_{ub2}$ and M_{lb1}, M_{lb2} are compared with the numerically calculated M (treated as the exact value of M) in Fig. 3.

To illustrate how the ratios among different semi-axis lengths affect the performance of the bounds of M, we also plot the relative errors of the bounds of M, i.e.,

$$\begin{aligned} e_{M_{ub}} &= (M_{ub} - M)/M, \\ e_{M_{lb}} &= (M_{lb} - M)/M, \end{aligned} \tag{43}$$

on a 2D grid plot, with the axes of b/a and c/a. Here, b/a and $c/a \in [1, 5]$, represent the ratios between the semi-axis lengths b, a and c, a, respectively (see Fig. 4). In all the trials, the errors of the bounds are less than 5 %. M_{lb1} and M_{ub1} always provide very tight bounds. M_{lb2} and M_{ub2} perform better when the triaxial ellipsoid is close to a uniaxial one, and for the uniaxial case, the error becomes absolute zero.

3.2.2 Surface area

The surface area of a triaxial ellipsoid with $a \le b \le c$ can be written exactly as [39]

$$F(a, b, c) = 2\pi\left(a^2 + \frac{ba^2}{\sqrt{c^2 - a^2}}F(\varphi, w) + b\sqrt{c^2 - a^2}\,E(\varphi, w)\right) \tag{44}$$

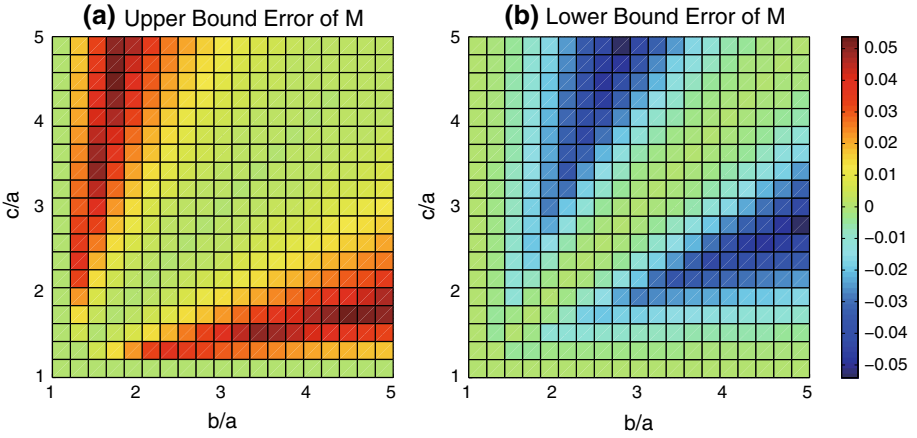

Fig. 4 With different aspect ratios of semi-axis lengths, errors of M_{ub} and M_{lb} are shown on a 2D grid plot, with the axes of b/a and c/a, where $b/a c/a \in [1, 5]$

where

$$w = \frac{c^2(b^2 - a^2)}{b^2(c^2 - a^2)} \text{ and } \varphi = \sin^{-1}\left(\sqrt{1 - \frac{a^2}{c^2}}\right).$$

Here $F(\varphi, w)$ and $E(\varphi, w)$ are respectively the incomplete elliptic integrals of the first and second kind. These integrals are built into packages such as Matlab, and values can be looked up efficiently. Nevertheless, it can be useful to evaluate bounds in terms of elementary functions.

$$F_{lb}(\partial C) \leq F(\partial C) \leq F_{ub}(\partial C). \tag{45}$$

Numerous papers provide lower and upper bounds on the surface area of ellipsoids [6,14, 39,40].

A convenient and very tighter upper bound of F can be found from the Cauchy–Schwartz inequality [35,37].

$$F_{ub1} = \frac{4\pi}{\sqrt{3}} \left(a^2b^2 + b^2c^2 + c^2a^2\right)^{\frac{1}{2}}. \tag{46}$$

Since the explicit formulas for the surface area of uniaxial ellipsoids are also known as follows. If $a = b = R$ and $c = \lambda R$ with $0 < \lambda < 1$, then [24]

$$F = 2\pi R^2 \left[1 + \frac{\lambda^2}{\sqrt{1 - \lambda^2}} \log\left(\frac{1 + \sqrt{1 - \lambda^2}}{\lambda}\right)\right].$$

When $\lambda > 1$,

$$F = 2\pi R^2 \left[1 + \frac{\lambda^2 \arccos(1/\lambda)}{\sqrt{\lambda^2 - 1}}\right].$$

We can also circumscribe a tightest uniaxial ellipsoid around a given triaxial ellipsoid as we did for M to obtain an upper bound of F, denoted as F_{ub2}.

Moreover, using the same "Schwartz-symmetrized" uniaxial ellipsoidal approximation, as what we did for M and the fact that $F(C^*) \leq F(C)$, we can obtain a tight lower bound of F, denoted as F_{lb}.

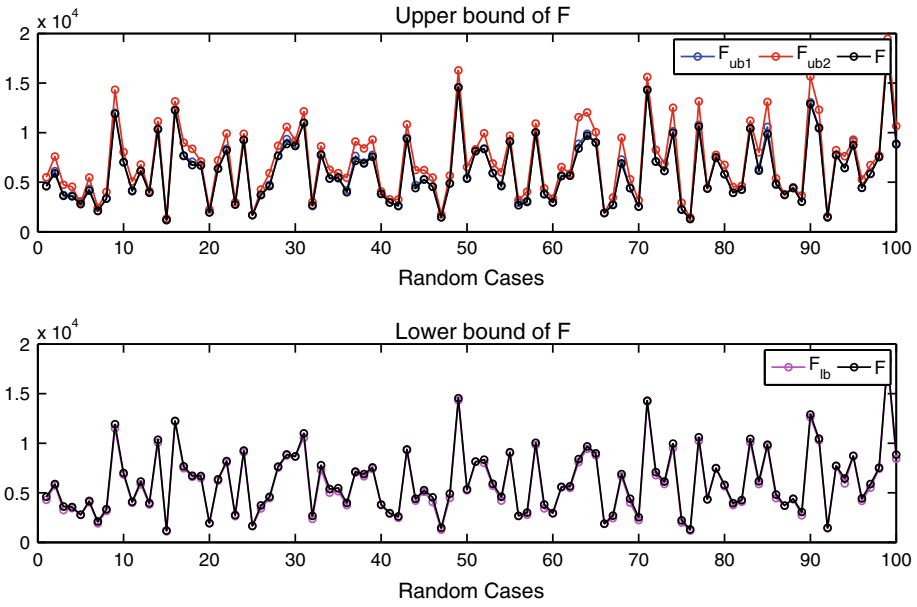

Fig. 5 *Upper* and *lower bounds*, F_{ub1}, F_{ub2} and F_{lb}, are compared with the exact values of F in 100 random trials, in which the semi-axis lengths and rotation angles of the ellipsoids are randomly sampled from uniform distributions $U[10, 50]$ and $U[0, 2\pi]$, respectively

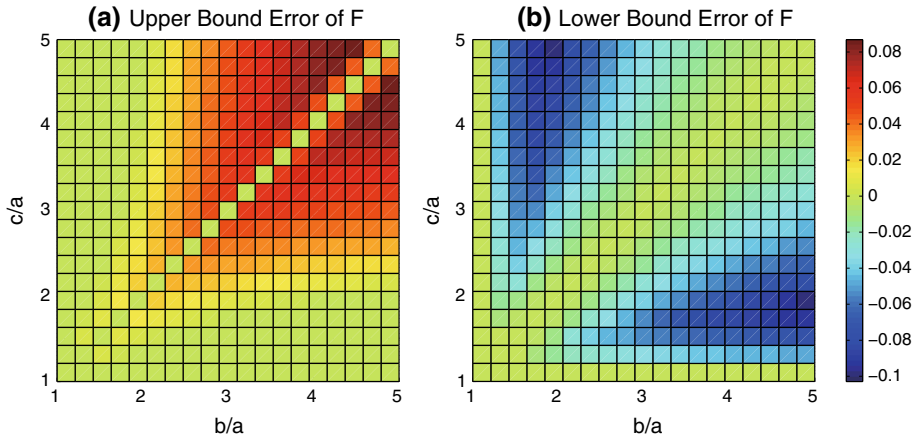

Fig. 6 With different aspect ratios of semi-axis lengths, errors of F_{ub} and F_{lb} are shown on a 2D grid plot, with the axes of b/a and c/a, where $b/a c/a \in [1, 5]$

To compare the results, we also use the same 100 random trials for F. The results of F_{ub1} F_{ub2} and F_{lb} are compared with the exact value of F in (44) in Fig. 5.

Similarly, we also plot the relative errors of the bounds of F, i.e.,

$$e_{F_{ub}} = (F_{ub} - F)/F, \qquad (47)$$
$$e_{F_{lb}} = (F_{lb} - F)/F,$$

on a 2D grid plot with the axes of b/a and c/a (see Fig. 6). Here,

$$F_{ub} = \max\{F_{ub1}, F_{ub2}\}. \tag{48}$$

Among all the trials, the errors of the bounds of F are always less than 10 %. The error becomes smaller when the triaxial ellipsoid is very close to a uniaxial one, and for the uniaxial case, the error becomes absolute zero.

3.3 Numerical comparison of bounds

This section evaluates the bounds derived in the previous sections. We begin with the planar case, and then address the spatial case.

3.3.1 Bounds for the planar case

For planar cases, we define bounds on the area enclosed by the Minkowski sum of ellipses as follows,

$$V_{BM} = \left(V(E_1)^{\frac{1}{2}} + V(E_2)^{\frac{1}{2}}\right)^{1/2}, \tag{49}$$

$$V_{lb} = \det(T)\left(V(C) + rL_{lb} + \pi r^2\right), \tag{50}$$

$$V_{ub} = \det(T)\left(V(C) + rL_{ub} + \pi r^2\right), \tag{51}$$

$$V_{exact} = \det(T)\left(V(C) + rL + \pi r^2\right), \tag{52}$$

where V_{BM} is a lower bound of the area from the *Brunn–Minkowski* inequality (10)). V_{lb} and V_{ub} are the lower and upper bounds from our Steiner's Formula-based approach. For planar cases, $V(C)$ becomes the area of the shrunk version of E_1 with semi-axis lengths $\tilde{a}_1$ and $\tilde{b}_1$, i.e.,

$$V(C) = \pi\tilde{a}_1\tilde{b}_1, \tag{53}$$

and $r = \min\{a_2, b_2\}$. $L_{lb}L_{ub}$ defined in (17), (18) and L defined in (14) are the upper, lower bounds and the exact formula for the perimeter of an ellipse, respectively. These are evaluated with the parameters $\tilde{a}_1$ and $\tilde{b}_1$ for the shrunk version of ellipse E_1.

Figure 7 illustrates the Minkowski sums of two ellipses in two different cases. Figure 8 shows the results of the relative errors for different bounds based on 100 trials, in which the semi-axis lengths and rotation angles of the ellipses are randomly sampled from uniform distributions $U[10, 50]$ and $U[0, 2\pi]$, respectively. The relative error k_m for different bounds is defined as $k_m = (V_m - V_{true})/V_{true}$. In Fig. 8, we can that see that V_{ub} and V_{lb} provide good upper and lower bounds with the relative errors less than 8 %. We note that V_{BM} always provides a much looser lower bound than V_{lb}. To avoid unnecessary scaling effect on the figure, we only plot V_{lb}, V_{ub} and V_{exact} in Fig. 8.

3.3.2 Bounds for the spatial case

For three-dimensional cases, V_{BM} [based on the *Brunn–Minkowski* inequality (10)], $V_{lb1}V_{ub1}$ and $V_{lb2}V_{ub2}$ are defined as follows,

$$V_{BM} = \left(V(E_1)^{\frac{1}{3}} + V(E_2)^{\frac{1}{3}}\right)^{1/3}, \tag{54}$$

$$V_{lb1} = \det(T)\left(V(C) + rF_{lb} + r^2M_{lb} + \tfrac{4\pi r^3}{3}\right), \tag{55}$$

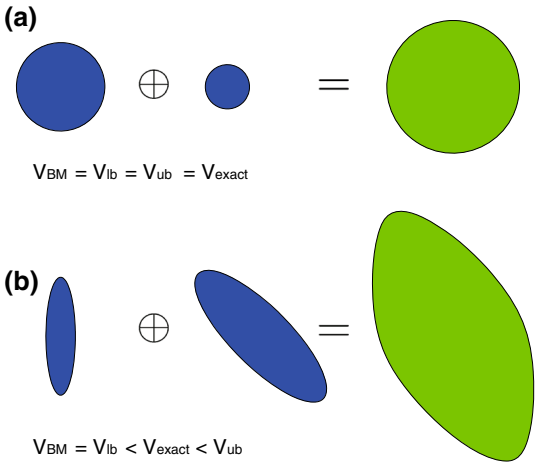

Fig. 7 Comparisons of different bounds and exact values of Minkowski sums of two ellipses in two different cases. **a** Both ellipses are circles with radius 3 and 1.5, respectively. In this case, $V_{BM} = V_{lb} = V_{ub} = V_{exact} = \pi(3 + 1.5)^3 = 63.61$. **b** The ellipses have semi-axis lengths 1, 5 and 3, 6, and rotation angles 0 and $\pi/4$, respectively. $V_{BM} = 131.9 < V_{lb} = 165.2 <= V_{exact} = 171.1 < V_{ub} = 179.1$

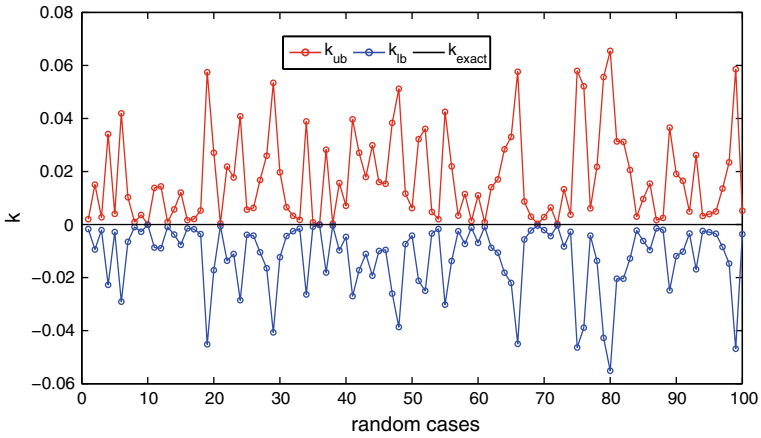

Fig. 8 The *upper* and *lower bounds*, V_{ub} and V_{lb}, compared with the exact value of the Minkowski-sum volumes of two ellipses, V_{exact}, based on 100 trials, in which the semi-axis lengths and angles of the ellipses are randomly sampled from uniform distributions $U[10, 50]$ and $U[0, 2\pi]$, respectively. The relative errors of the *upper* and *lower bounds*, k_{ub} and k_{lb}, are calculated and shown in the figure. Here, $k_{exact} = 0$

$$_{ub1} = \det(T)\left(V(C) + rF_{ub} + r^2 M_{ub} + \tfrac{4\pi r^3}{3}\right), \tag{56}$$

$$_{lb2} = \det(T)\left(V(C) + rF + r^2 M_{lb} + \tfrac{4\pi r^3}{3}\right), \tag{57}$$

$$_{ub2} = \det(T)\left(V(C) + rF + r^2 M_{ub} + \tfrac{4\pi r^3}{3}\right), \tag{58}$$

$$_{exact} = \det(T)\left(V(C) + rF + r^2 M + \tfrac{4\pi r^3}{3}\right), \tag{59}$$

where $V(C)$ is the volume of the shrunk version of E_1, with semi-axis lengths $\tilde{a}_1\tilde{b}_1$ and $\tilde{c}_1$, i.e.,

$$V(C) = \frac{4\pi}{3}\tilde{a}_1\tilde{b}_1\tilde{c}_1, \tag{60}$$

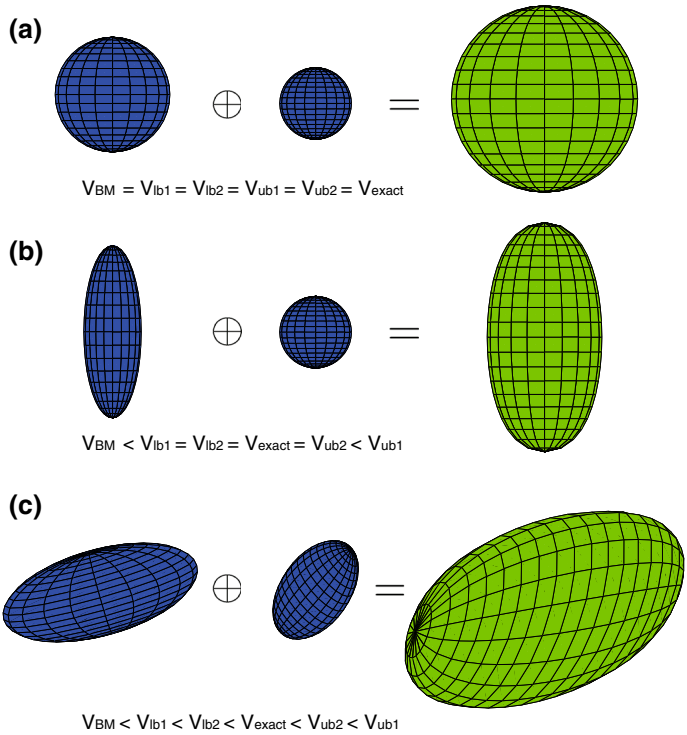

Fig. 9 Comparisons of different bounds and exact values of Minkowski sums of two ellipsoids in three different cases. **a** Both ellipsoids are spherical balls with radius 4 and 2.5, respectively. In this case, $V_{BM} = V_{lb1} = V_{lb2} = V_{exact} = V_{ub2} = V_{ub1} = \frac{4\pi}{3}(4+2.5)^3 = 1.15 \times 10^3$. **b** One ellipsoid is a spherical ball with radius 2, the other one is axis-symmetric with semi-axis lengths 2, 2, 6. $V_{BM} = 448.1 < V_{lb1} = V_{lb2} = V_{exact} = V_{ub2} = 563.3 < V_{ub1} = 573.7$. **c** Both ellipsoids are triaxial with semi-axis lengths as 7, 3, 3 and 2, 3, 4, and ZXZ Euler angles as $-\pi/4, -pi/8, \pi/4$ and $\pi/3, \pi/4, -\pi/6$, respectively. $V_{BM} = 1354.4 < V_{lb1} = 1678.8 < V_{lb2} = 1724.3 < V_{exact} = 1725.9 < V_{ub2} = 1729.2 < V_{ub1} = 1741.2$

and $r = \min\{a_2, b_2, c_2\}$. After calculating the offset surface, the "stretching" operation T can be found in (9). F is defined in (44) as the exact surface area and the exact value of the total mean curvature M is calculated numerically based on (26). $M_{lb}M_{ub}$ and $F_{lb}F_{ub}$ are the best lower and upper bounds of the total mean curvature and the surface area, respectively. V_{lb1} and V_{ub1} use bounds for both M and F, while V_{lb2} and V_{ub2} use the exact value of F and the bounds of M. These are all evaluated with the parameters $\tilde{a}_1\tilde{b}_1\tilde{c}_1$ for the shrunk version of ellipse E_1.

Figure 9 illustrates the Minkowski sums of two ellipsoids in three different cases. Figure 10 shows the results of the relative errors for different bounds based on 100 trials, in which the semi-axis lengths and rotation angles of the ellipsoids are randomly sampled from uniform distributions $U[10, 50]$ and $U[0, 2\pi]$, respectively. With our best bounds of M and F, the relative errors of the Minkowski-sum volumes can be bounded by 6 %. With the best bounds of M and the exact value of F calculated in closed form in (44), the relative errors can be further reduced and bounded by 2 %.

3.4 Volume estimates derived from bounds

In addition to exact lower and upper bounds on the volume of Minkowski sums of ellipsoids based on our parametric description, we consider estimates of the volume. Two immediate

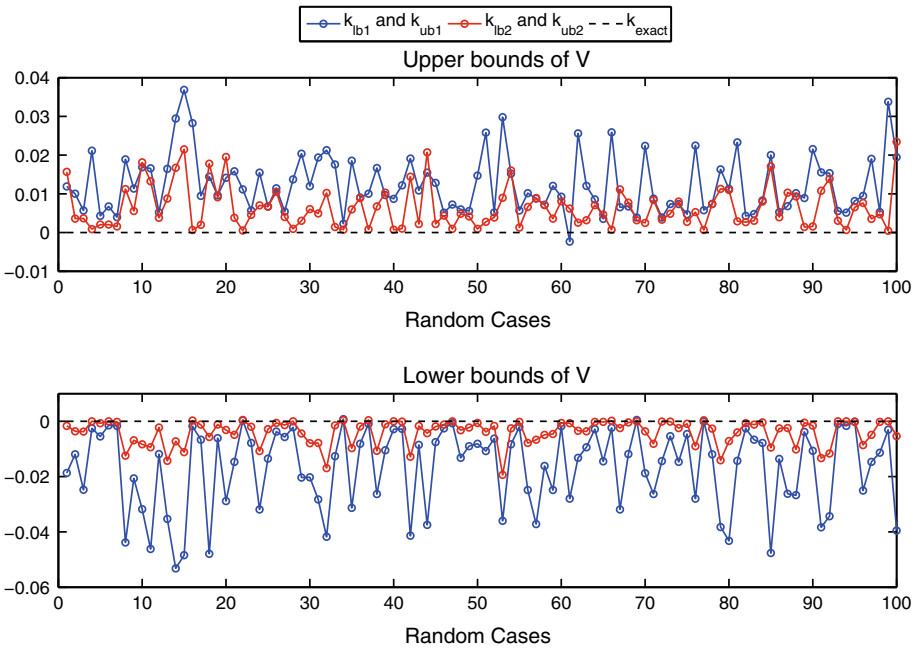

Fig. 10 The *upper* and *lower bounds*, $V_{ub1}V_{ub2}V_{lb1}$ and V_{lb2}, are compared with the exact value of the Minkowski-sum volumes, V_{exact}, based on 100 trials, in which the semi-axis lengths and angles of the ellipses are randomly sampled from uniform distributions $U[10, 50]$ and $U[0, 2\pi]$, respectively. The relative errors of these bounds, $k_{ub1}k_{ub2}k_{lb1}$ and k_{lb2}, are calculated and shown in the figure. Here, $k_{exact} = 0$

estimates are obtained from taking the arithmetic and geometric means of our best lower and upper bounds V_{lb1} and V_{ub1}, induced by our best bounds of M and F:

$$V_{AM} = \frac{1}{2}(V_{lb1} + V_{ub1}), \tag{61}$$

$$V_{GM} = \sqrt{V_{lb1} \cdot V_{ub1}}. \tag{62}$$

From the AM-GM inequality, $V_{GM} \leq V_{AM}$.

Other estimates can be obtained by replacing the lower and upper bounds on F (Fig. 12), or in the planar case, L (Fig. 11) with their estimates.

For example, a modified Ramanujan approximation of the perimeter of an ellipse with $a \leq b$ is [42]

$$L_{est} = \pi(a+b)\left(1 + \frac{3(b-a)^2/(b+a)^2}{10 + \sqrt{4 - 3(b-a)^2/(b+a)^2}}\right). \tag{63}$$

An approximate formula for the area of a triaxial ellipsoid has been given recently (by Thomsen and Cantrell independently) as [1]

$$F_{est} = 4\pi\left(\frac{a^p b^p + a^p c^p + b^p c^p}{3}\right)^{1/p} \quad \text{where} \quad p = 1.6075. \tag{64}$$

With

$$M_{est} = \frac{1}{2}(M_{lb} + M_{ub}), \tag{65}$$

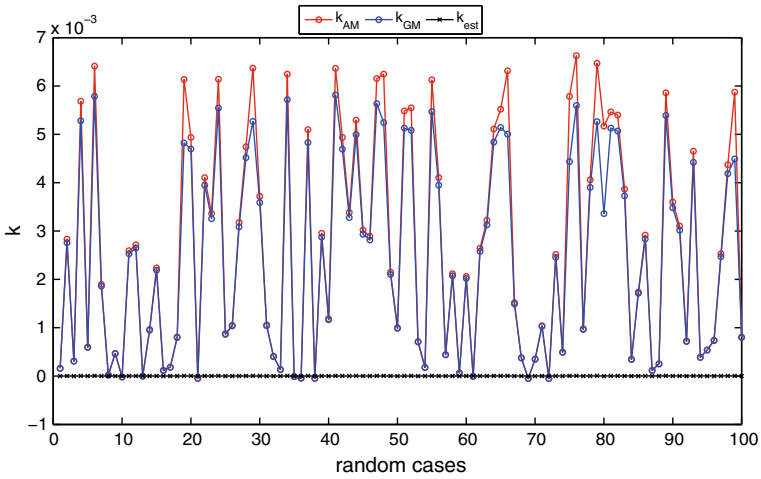

Fig. 11 The relative errors of different area estimates, $V_{AM}\,V_{GM}$ and V_{est}, for $E_1 \oplus E_2$ are calculated based on 100 trials, in which the semi-axis lengths and angles of the ellipses are randomly sampled from uniform distributions $U[10, 50]$ and $U[0, 2\pi]$, respectively

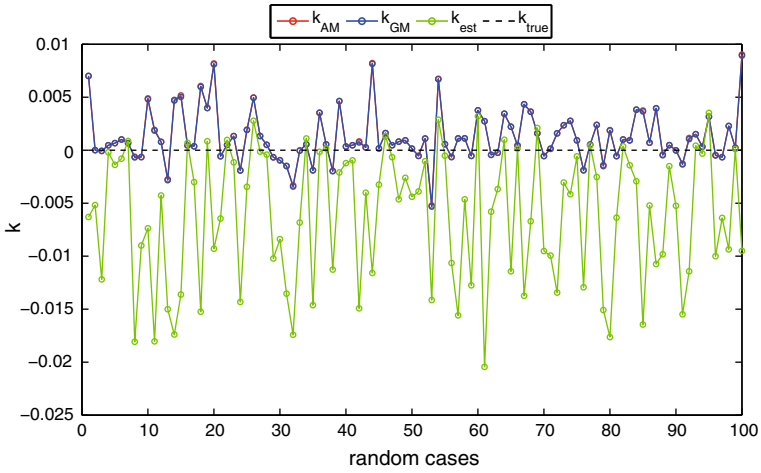

Fig. 12 The relative errors of different volume estimates, $V_{AM}\,V_{GM}$ and V_{est}, for $E_1 \oplus E_2$ are calculated based on 100 trials, in which the semi-axis lengths and angles of the ellipsoids are randomly sampled from uniform distributions $U[10, 50]$ and $U[0, 2\pi]$, respectively

these can be used in Steiner's formula to obtain an estimate of the volume within an offset of an ellipse or ellipsoid.

The relative errors of the estimated volumes $V_{AM}\,V_{GM}$ and V_{est} of the 2D and 3D cases are compared in Figs. 11 and 12. In planar cases, the relative errors of V_{est} provides a very accurate estimation, i.e., $k_{est} \approx 0$. V_{AM} and V_{GM}, computed from our best lower and upper bounds V_{lb1} and V_{ub1}, are very good estimations as well, with the relative errors bounded by 0.7 %. In spatial cases, the relative errors of V_{est} become larger. V_{AM} and V_{GM} in this case provide better estimations, with the relative errors always less than 1 %.

4 A kinematic formula for containment

In classical integral geometry, the Principal Kinematic Formula plays a central role. The formula expresses the average Euler characteristic of the intersections of rigid bodies moving uniformly at random in terms of fundamental quantities of these bodies (volume, area, etc.). When the bodies are convex, the intersections are convex, and the Euler characteristic can be replaced by the set indicator function, $\iota(\cdot)$ which takes a value of 1 when the argument is nonempty, and 0 otherwise. The resulting formula works in $\mathbb{R}^n$ and has been extended to general spaces of constant curvature. But we are concerned only with two- and three-dimensional Euclidean space, in which case the result is in the following subsections.

4.1 Planar cases

Theorem 1 ([7,8,38]) *Given convex bodies C_0 and C_1 in $\mathbb{R}^2$, then*

$$\int_{SE(2)} \iota(C_0 \cap gC_1)\, dg = 2\pi[V(C_0) + V(C_1)] + L(\partial C_0) \cdot L(\partial C_1). \tag{66}$$

where $V(\cdot)$ is the area of the planar body and $L(\cdot)$ is its circumference. In $\mathbb{R}^3$

$$\int_{SE(3)} \iota(C_0 \cap gC_1)\, dg = 8\pi^2[V(C_0) + V(C_1)] + 2\pi\,[F(\partial C_0)M(\partial C_1) + F(\partial C_1)M(\partial C_0)] \tag{67}$$

where $F(\cdot)$ and $M(\cdot)$ are respectively the area and integral of mean curvature of the surface enclosing the body, and $V(\cdot)$ is the volume of the body. In these equations, $SE(n)$ denotes the $(n+1)n/2$-dimensional Lie group of proper rigid-body motions in n-dimensional Euclidean space, and dg denotes its (unnormalized) Haar measure. For the proof and pointers to the literature, see [7,8,29,43–45,47].

An alternative proof specifically for convex bodies was given in [13]. In that proof, the center of the moving body, C_1, visits every point in the fixed body, C_0, and rotates freely, each time contributing to the integral, and resulting in the $2\pi V(C_0)$ and $8\pi^2 V(C_0)$ terms. Then, the moving body is decomposed into concentric shells, and as each shell makes every possible point contact with the boundary ∂C_0, intersections of the original bodies is also guaranteed. Adding up these contributions results in the above formulas.

This alternative proof is mentioned, because a new kind of kinematic formula can be derived in essentially the same way. In this new formula, we are concerned not with measuring the volume in $SE(n)$ corresponding to all possible intersections of bodies, but rather the integral of the volume in $SE(n)$ corresponding to all possible ways that C_1 can move while being fully contained in C_0. To this end, let $b(gC_1 \subset C_0)$ take a value of 1 when $gC_1 \subset C_0$ and a value of zero otherwise, corresponding to the binary truth of the statement that the moving body is fully contained in the stationary one.

Theorem 2 *Given convex bodies C_0 and C_1 in $\mathbb{R}^n$ for $n = 2, 3$ such that C_0 can be written as the Minkowski sum $C_0'(R) \oplus RC_1$ for any $R \in SO(n)$ where $C_0'(R)$ is a convex body that depends on R, then*

$$\int_{SE(2)} b((g \cdot C_1) \subset C_0)\, dg = 2\pi[V(C_0) + V(C_1)] - L(\partial C_0) \cdot L(\partial C_1) \tag{68}$$

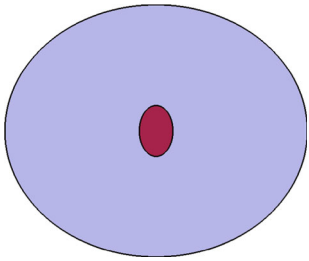

Fig. 13 A planar example when one ellipse can move freely at all the orientations inside another without collision and it is desirable to compute the free room to move

and

$$\int_{SE(3)} b((g \cdot C_1) \subset C_0)\, dg \tag{69}$$
$$= 8\pi^2[V(C_0) - V(C_1)] - 2\pi F(\partial C_0)M(\partial C_1) + 2\pi F(\partial C_1)M(\partial C_0).$$

For example, if C_0 and C_1 are circular disks in the plane with radii $r_0 > r_1$, then $L(\partial C_i) = 2\pi r_i V(\partial C_i) = \pi r_i^2$ and the above planar formula (68) gives $2\pi^2(r_0 - r_1)^2$, which is 2π times the area of a disk of radius $r_0 - r_1$. Similarly, in the 3D case where $F(\partial C_i) = 4\pi r_i^2 M(\partial C_i) = 4\pi r_i V(C_i) = \frac{4}{3}\pi r_i^3$, the above 3D formula (70) gives $8\pi^2$ times the volume enclosed by a sphere of radius $r_0 - r_1$.

We know of no other work that addresses this problem. The closest works are those of Zhou [51–54] that address when one body can be contained within another (but not the amount of motion allowed for a contained body). In some practical engineering contexts, this can be quite important [9,11,27].

Figure 13 illustrates a planar example with the semi-axis lengths of E_1 and E_2 are 18, 15 and 2, 3, respectively. We numerically calculated the sum of all volumes of the Minkowski difference of two ellipses when one can move freely at all the orientations inside another without collision. The relationship between the result of Theorem 2 and the main topic of this paper is that

$$V_{num} = \int_{SE(2)} b\left((g \circ E_1) \subset E_0\right) dg = \int_{SO(2)} V\left(E_0 \ominus (g \circ E_1)\right) dg. \tag{70}$$

In the example of Fig. 13, we compare V_{num} with V_{PK}, the volume calculated based on (68). The result shows that $V_{num} = V_{PK} = 3.799 \times 10^3$.

4.2 Spatial cases

The subject of translative kinematic formulas for general bodies that compute integrals of the form $\int_{\mathbb{R}^n} \iota(C_0 \cap tC_1)\, dt$ for convex bodies has been addressed extensively in [15,16,18,20,21,46,49,50]. Using our method, given ellipsoidal bodies E_0 and E_1 with

$$a_1 \le b_1 \le c_1 \le a_0 \le b_0 \le c_0$$

we can compute a translative integral geometric formula for containment of the form

$$\int_{\mathbb{R}^n} b\left(tE_1 \subset E_0\right) dt = V\left(E_0 \ominus E_1\right).$$

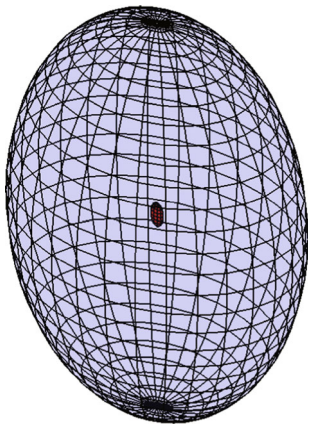

Fig. 14 A spatial example when one ellipsoid can move freely at all the orientations inside another without collision

The result of this formula is related to the formulas given in the previous section because

$$\int_{SE(3)} b\left((g \cdot E_1) \subset E_0\right) dg = \int_{SO(3)} V\left(E_0 \ominus (R \cdot E_1)\right) dR.$$

But by using our closed-form translative kinematic formula for containment (which uses the Minkowski sum and difference results from earlier in the paper), we can also compute what the volume of motion is in $SE(3)$ when the range of rotations is restricted.

Figure 14 illustrates a 3D example with the semi-axis lengths of E_1 and E_2 are 30, 40, 50 and 1, 2, 3, respectively. In this case, V_{num} is defined as

$$V_{num} = \int_{SO(3)} V(E_0 \ominus (R \cdot E_1)) dR. \tag{71}$$

In this 3D example, we also compared V_{num} with V_{PK} [based on (69)] numerically. However, it is only feasible to discretize the 3D space of $SO(3)$ coarsely, and hence cross-validation is only approximate. With the resolution of integration in each degree of freedom defined by 50 sample points, we have $V_{num} = 1.57 \times 10^7$ and $V_{PK} = 1.64 \times 10^7$, which verifies to within discretization error that these quantities are the same.

We note that if an ellipsoidal robot navigates within an ellipsoidal arena containing ellipsoidal obstacles, the methodology presented above can be used to compute the volume of collision-free motion in $SE(n)$ when certain conditions hold. In particular, if the obstacles are small enough and placed far enough away from the boundary of the arena such that it is never possible for the robot to simultaneously intersect two or more obstacles or an obstacle and the boundary of the arena, then the volume of motions computed from our containment formula can be computed first, and then the volume of motions computed from the Principal Kinematic Formula for the robot and each obstacle can be computed and subtracted. The result will be the volume of free motion. If the conditions mentioned above regarding the size and distribution of obstacles does not hold, then the result computed in this way will be an upper bound on the free motion. Moreover, using our bounds on the volume of Minkowski sums and differences, analogous quantities can be computed for the pure translative case (under less restrictive conditions on the size and location of obstacles).

5 Conclusion

In this paper, we derive closed-form parametric expressions for the exact boundaries of the Minkowski sum and difference of two solid ellipsoidal bodies oriented arbitrarily in n-dimensional Euclidean space. In contrast with existing methods, our approaches are completely analytical and have closed forms. With our exact parameterization, the volumes of the Minkowski sum and difference of two ellipsoids can be numerically calculated efficiently. For even faster evaluation of these volumes, we develop a method based on Steiner's Formula to provide tight upper and lower bounds. These bounds deviate from the actual values only by a few percent over a wide range of aspect ratios and orientations. In the context of a robotics application we also illustrate the relationship between the Principal Kinematic Formula, a related containment formula, and the volume bounds that we obtain for the Minkowski sums and differences of ellipsoids.

Acknowledgments This work was performed while the authors were supported under NSF Grant IIS-1162095. We would like to thank Mr. Joshua Davis, Mr. Qianli Ma, and the anonymous reviewer for their comments.

References

1. http://www.numericana.com/answer/ellipsoid.htm#thomsen (2006)
2. Agarwal, P.K., Flato, E., Halperin, D.: Polygon decomposition for efficient construction of Minkowski sums. Comput. Geom. **21**(1–2), 39–61 (2002). doi:10.1016/S0925-7721(01)00041-4
3. Alfano, S., Greer, M.L.: Determining if two solid ellipsoids intersect. J. Guid. Control Dyn. **26**(1), 106–110 (2003). http://cat.inist.fr/?aModele=afficheN&cpsidt=14481669
4. Bajaj, C.L., Kim, M.-S.: Generation of configuration space obstacles: the case of moving algebraic curves. Algorithmica **4**(1–4), 157–172 (1989)
5. Behar, E., Lien, J.-M.: Dynamic Minkowski sum of convex shapes. In: Robotics and Automation (ICRA), 2011 IEEE International Conference on. IEEE, pp. 3463–3468 (2011)
6. Behar, E., Lien, J.-M.: Dynamic Minkowski sum of convex shapes. In: 2011 IEEE International Conference on Robotics and Automation, pp. 3463–3468. IEEE (2011). http://ieeexplore.ieee.org/xpl/articleDetails.jsp?arnumber=5979992
7. Blaschke, W.: Einige bemerkungen über kurven und flächen konstanter breite. Leipz. Ber. **57**, 290–297 (1915)
8. Blaschke, W.: Vorlesungen über Integralgeometrie. VEB Dt. Verlag d. Wiss (1955)
9. Boothroyd, G., Redford, A.H.: Mechanized Assembly: Fundamentals of Parts Feeding, Orientation, and Mechanized Assembly. McGraw-Hill, New York (1968)
10. Chan, K., Hager, W.W., Huang, S.-J., Pardalos, P.M., Prokopyev, O.A., Pardalos, P.: Multiscale Optimization Methods and Applications, ser. Nonconvex Optimization and Its Applications, vol. 82. Kluwer, Boston (2006). http://www.springerlink.com/content/x427m4u6313241p4/
11. Chirikjian, G.S.: Parts entropy and the principal kinematic formula. In: Automation Science and Engineering: CASE 2008. IEEE International Conference on, pp. 864–869. IEEE 2008 (2008)
12. Chirikjian, G.S.: Stochastic Models, Information Theory, and Lie Groups, Volume 1: Analytic Methods and Modern Applications, vol. 1. Birkhäuser, Boston (2009)
13. Chirikjian, G.S.: Stochastic Models, Information Theory, and Lie Groups, Volume 2: Analytic Methods and Modern Applications, vol. 1. Birkhäuser, Boston (2011)
14. Fogel, E., Halperin, D.: Exact and efficient construction of Minkowski sums of convex polyhedra with applications. Comput.-Aided Des. **39**(11), 929–940 (2007). http://linkinghub.elsevier.com/retrieve/pii/S0010448507001492
15. Glasauer, S.: A generalization of intersection formulae of integral geometry. Geom. Dedic. **68**(1), 101–121 (1997)
16. Glasauer, S.: Translative and kinematic integral formulae concerning the convex hull operation. Math. Z. **229**(3), 493–518 (1998)
17. Goldman, R.: Curvature formulas for implicit curves and surfaces. Comput. Aided Geom. Des. **22**(7), 632–658 (2005)

18. Goodey, P., Weil, W.: Translative integral formulae for convex bodies. Aequ. Math. **34**(1), 64–77 (1987)
19. Goodey, P., Weil, W.: Intersection bodies and ellipsoids. Mathematika **42**(02), 295–304 (1995). http://journals.cambridge.org/abstract_S0025579300014601
20. Goodey, P., Well, W.: Intersection bodies and ellipsoids. Math. Lond. **42**, 295–304 (1995)
21. Groemer, H.: On translative integral geometry. Arch. Math. **29**(1), 324–330 (1977)
22. Guibas, L., Ramshaw, L., Stolfi, J.: A kinetic framework for computational geometry. In: Proceedings of the 24th Annual IEEE Symposium Foundations of Computer Science, pp. 100–111 (1983)
23. Hachenberger, P.: Exact Minkowksi sums of polyhedra and exact and efficient decomposition of polyhedra into convex pieces. Algorithmica **55**(2), 329–345 (2008). http://dl.acm.org/citation.cfm?id=1554962.1554966
24. Hadwiger, H.: Altes und Neues ü ber konvexe Körper. Birkhäuser, Basel (1955)
25. Halperin, D., Latombe, J.-C., Wilson, R.H.: A general framework for assembly planning: the motion space approach. Algorithmica **26**(3–4), 577–601 (2000)
26. Hartquist, E., Menon, J., Suresh, K., Voelcker, H., Zagajac, J.: A computing strategy for applications involving offsets, sweeps, and Minkowski operations. Comput.-Aided Des. **31**(3), 175–183 (1999).10.1016/S0010-4485(99)00014-7
27. Karnik, M., Gupta, S.K., Magrab, E.B.: Geometric algorithms for containment analysis of rotational parts. Comput.-Aided Des. **37**(2), 213–230 (2005)
28. Kaul, A., Farouki, R.T.: Computing minkowski sums of plane curves. Int. J. Comput. Geom. Appl. **5**(04), 413–432 (1995)
29. Klain, D.A., Rota, G.-C.: Introduction to Geometric Probability. University Press, Cambridge (1997)
30. Klamkin, M.: Elementary approximations to the area of n-dimensional ellipsoids. Am. Math. Mon. **78**(3), 280–283 (1971)
31. Kurzhanskiĭ, A., Vályi, I.: Ellipsoidal Calculus for Estimation and Control. In: Birkhäuser Mathematics, vol. **XV** (1994)
32. Kurzhanskiy, A.A., Varaiya, P.: Ellipsoidal toolbox (et). In: Decision and Control, 2006 45th IEEE Conference on. IEEE, pp. 1498–1503 (2006)
33. Latombe, J.-C.: Robot Motion Planning. Kluwer, Dordrecht (1990)
34. Lee, I.-K., Kim, M.-S., Elber, G.: Polynomial/rational approximation of minkowski sum boundary curves. Graph. Models Image Process. **60**(2), 136–165 (1998)
35. Lehmer, D.H.: Approximations to the area of an n-dimensional ellipsoid. Can. J. Math. **2**, 267–282 (1950)
36. Perram, J. W., Wertheim, M.: Statistical mechanics of hard ellipsoids. I. Overlap algorithm and the contact function. J. Comput. Phys. **58**(3), 409–416 (1985). doi:10.1016/0021-9991(85)90171-8
37. Pfiefer, R.: Surface area inequalities for ellipsoids using Minkowski sums. Geom. Dedic. **28**(2), 171–179 (1988). http://link.springer.com/10.1007/BF00147449
38. Poincaré, H.: Calcul de Probabilités, 2nd edn. Paris (1912)
39. Rivin, I.: Surface area and other measures of ellipsoids. Adv. Appl. Math. **39**(4), 409–427 (2007). http://linkinghub.elsevier.com/retrieve/pii/S019688580700070X
40. Ros, L., Sabater, A., Thomas, F.: An ellipsoidal calculus based on propagation and fusion. Syst. Man Cybern. Part B Cybern. IEEE Trans. **32**(4), 430–442 (2002)
41. Sack, J.-R., Urrutia, J.: Handbook of Computational Geometry. North Holland, Amsterdam (1999)
42. Salomon, D.: Curves and Surfaces for Computer Graphics. Springer, New York (2006)
43. Santaló, L.A.: Integral Geometry and Geometric Probability. Cambridge University Press, Cambridge, MA (2004)
44. Schneider, R.: Kinematic measures for sets of colliding convex bodies. Mathematika **25**(01), 1–12 (1978)
45. Schneider, R.: Integral geometric tools for stochastic geometry. In: Lecture Notes in Mathematics. Springer, Berlin (2007)
46. Schneider, R., Weil, W.: Translative and kinematic integral formulae for curvature measures. Math. Nachr. **129**(1), 67–80 (1986)
47. Schneider, R., Weil, W.: Stochastic and Integral Geometry. Springer, Berlin (2008)
48. Stoyan, D., Kendall, W. S., Mecke, J., Kendall, D.: Stochastic Geometry and its Applications, vol. 8. Wiley Chichester (1987)
49. Weil, W.: Translative integral geometry. Geobild **89**, 75–86 (1989)
50. Weil, W.: Translative and kinematic integral formulae for support functions. Geom. Dedic. **57**(1), 91–103 (1995)
51. Zhang, G.: A sufficient condition for one convex body containing another. Chin. Ann. Math. Ser. B **9**(4), 447–451 (1988)
52. Zhou, J.: A kinematic formula and analogues of hadwiger's theorem in space. Contemp. Math. **140**, 159–159 (1992)

53. Zhou, J.: When can one domain enclose another in r^3? J. Aust. Math. Soc. Ser. A **59**(2), 266–272 (1995)
54. Zhou, J.: Sufficient conditions for one domain to contain another in a space of constant curvature. Proc. Am. Math. Soc. **126**(9), 2797–2803 (1998)